# Effects of drugs covalent binding on DNA: joint use of microRaman spectroscopy and HRTEM imaging

Spectrochimica Acta Part A: Molecular and Biomolecular Spectroscopy 343 (2025) 126606

Contents lists available at ScienceDirect

Spectrochimica Acta Part A:
Molecular and Biomolecular Spectroscopy

journal homepage: www.journals.elsevier.com/spectrochimica-acta-part-a-molecular-and-biomolecular-spectroscopy

# Effects of drugs covalent binding on DNA: joint use of microRaman spectroscopy and HRTEM imaging☆

Monica Marini [a,*], Bruno Torre [a,b], Emanuele Bosurgi [b], Marco Allione [b], Candido Fabrizio Pirri [b], Enzo di Fabrizio [b,**]

[a] Istituto Nazionale di Ricerca Metrologica (INRiM), Strada delle Cacce 91, 10135 Torino, Italy
[b] Department of Applied Science and Technologies (DISAT), Politecnico di Torino, 10129 Torino, Italy

## HIGHLIGHTS

- Drugs bind to DNA to induce structural and chemical changes.
- Superhydrophobic devices enable background-, label-free study of DNA-drug adducts.
- Physiological and altered DNA state are identified by fine Raman spectra variations.
- HRTEM direct imaging confirms DNA local denaturation upon drug exposure.

## GRAPHICAL ABSTRACT

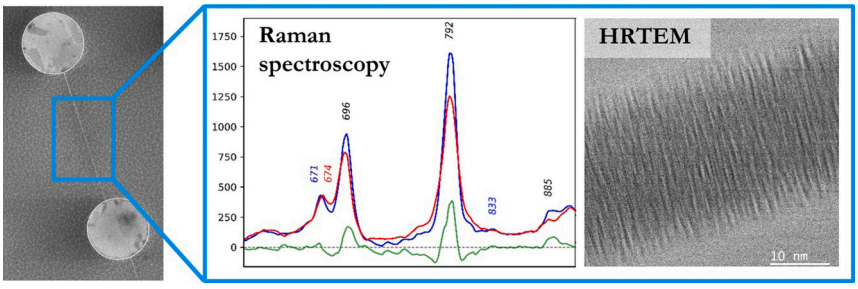


## ARTICLE INFO

*Keywords:*
Suspended cisplatin-DNA filaments
microRaman spectroscopy
High-resolution transmission electron microscopy
Superhydrophobicity

## ABSTRACT

The detailed understanding of drugs interaction with cells biomolecules is fundamental to evaluate the most efficient drug dosage. In this work we provide details on the structural modification occurring to DNA upon cross-links formation with metal ions after the administration of chemotherapeutic compounds. We used nanometric filaments of suspended DNA on superhydrophobic-based devices (SHS) for an accurate analysis by microRaman spectroscopy and high-resolution transmission electron microscopy (HRTEM) to study the interaction of cisplatin with the double helix. Our data show a conformational transition of the nucleic acids upon drugs administration, relying on Raman shift and intensity variations to features such as backbone vibration (792, 834 $cm^{-1}$), guanine ring breathing (~670 $cm^{-1}$), stretching modes of the adenine ring (~1300 $cm^{-1}$, 1338 $cm^{-1}$), unpaired AT bases (1178 $cm^{-1}$ and 1204 $cm^{-1}$) and deoxyribosyl CH stretching vibrations (range 2800–3000 $cm^{-1}$). The conformational transitions towards a loosen DNA form and the integration of the drug into the double helix structures has been further confirmed by HRTEM, describing local helix denaturation. We demonstrated that the proposed methodology can be used to distinguish treated from pristine DNA by their Raman spectra, confirmed by the structural insights provided by direct imaging.

☆ This article is part of a Special issue entitled: 'ECSBM2024' published in Spectrochimica Acta Part A: Molecular and Biomolecular Spectroscopy.

* Corresponding author at: Istituto Nazionale di Ricerca Metrologica (INRiM), Strada delle Cacce 91, 10135 Torino, Italy.
** Corresponding author.
*E-mail addresses:* m.marini@inrim.it (M. Marini), enzo.difabrizio@polito.it (E. di Fabrizio).

https://doi.org/10.1016/j.saa.2025.126606
Received 28 March 2025; Received in revised form 5 June 2025; Accepted 23 June 2025
Available online 25 June 2025

## 1. Introduction

Cisplatin [cis-diammine-dichloroplatinum(II)] is the first metal-based anticancer drug approved by the Food and Drug Administration (FDA) in 1978 [1]. Since then, it has been used in the treatment of several types of cancers such as testicular cancer, ovarian cancer, lung cancer, and childhood brain tumors among others [2]. Cisplatin becomes active towards nucleic acids only upon the uptake and internalization in the cell and the anticancer effect is actuated via the formation of adducts with double-strand DNA in the nucleus [2]. Due to the lower chlorine concentration, cisplatin chlorine moieties can be released in favor of the complexation with up to two molecules of water [3]. Activated cisplatin then forms three main types of structures with DNA in a process named 'platination': mono adducts, intrastrand crosslinks and interstrand crosslinks [4]. Monoadduct formation is mainly transient as it is further converted into intra- and inter-strand crosslinks. The favored platination event allows the formation of intrastrand crosslinks in the 90 % of the cases and a cisplatin molecule is covalently bound to two nucleotides on the same strand [5]. In intrastrand crosslinking, cisplatin interacts with the nucleophilic residues of the bases, more precisely with the N7 atom of neighboring purine residues (1,2-GpG and 1,2-⟩GpA) [6]. This alteration promotes the anticancer effects of the drug [7] by triggering cell death [8,9]. For these reasons, the detailed understanding of the structural modifications induced by the interaction with its biological targets, which is at the basis of drug efficiency [10], resistance [11] and side effects, is crucial for the development of a personalized therapy and to determine the molecular processes behind the action of drugs.

Several studies focus on the relation between the structure of the complex drug-DNA and the cisplatin-nucleotide ratio and were carried out with well-established structural and spectroscopic techniques [12–14]. Conventional techniques such as X-ray diffraction [15–17], and Nuclear Magnetic Resonance [5,18,19], focused on the study of oligonucleotides and were of fundamental importance in resolving the structure of cisplatin-DNA adducts and in the assessment of the kinetics of the platination process. Crystallographic techniques have confirmed the binding geometry of cisplatin to the N7 position of guanine, as well as the intermolecular interactions between the ammine groups of cisplatin and the neighboring phosphate oxygen atoms [15]. These studies also revealed the significant alteration of the DNA double helix upon drug binding [17]. Notably, discrepancies were observed between structural data obtained from different techniques [12]. While NMR spectroscopy indicated severe distortions of the helical axis and an overall strained system, it consistently identifies the DNA as adopting a canonical B-form conformation; on the other hand, X-ray crystallography revealed the presence of both A- and B-form features within the same structure [17]. This divergence is generally attributed to crystal packing effects, which may stabilize high-energy conformational states that are unlikely to be populated under physiological conditions [12].

Raman spectroscopy studies on DNA identified several characteristic marker bands associated with different conformational states, as well as vibrational modes arising from the various nucleobases and organic moieties of specific nucleotides and their interactions [20–22]. In the specific case of cisplatin–DNA interactions, spontaneous Raman spectroscopy has revealed structural alterations in the DNA, primarily associated with a partial transition from B-form to A-form. Raman spectral signatures indicative of cisplatin binding at the N7 position of guanine have been observed, along with features consistent with DNA melting and pre-melting transitions [13,23–25].

DNA-ligand interactions were studies also by Surface-Enhanced Raman Spectroscopy (SERS), which is a highly sensitivity technique due to the plasmonic enhancement allowed by metallic nanostructures [26,27]. However, it is important to note that for extended molecules such as DNA, the SERS signal strongly depends on the fraction of the molecule in direct contact with the plasmonic substrate. As a result, significant spectral variability can arise between different measurements [28].

A consistent relation between sample preparation and spectroscopic signal has been also described [29]. It has to be noted that these investigations are based on the use of short-chained oligonucleotides, in the range of hundreds of base pairs, and therefore composed by a limited number of bases, which are not representative of the information dispersed through a cellular native DNA molecule [5,13–15,18,19]. Spectroscopic techniques, in particular Raman spectroscopy, have extended the analytical capabilities to longer DNA molecules (up to 2000–4000 bp) giving structural and chemical information about the variety of structure formed as well as their dynamics [30–33]. Nevertheless, the time-consuming preparation procedures needed to obtain the amount and the purity of material for adduct analysis is a limiting factor for their routinary application in the detection and description of structural alterations. Also, the type of preparation procedure affects the sample response itself. For instance, several spectroscopic studies used macroscopic samples such as crystals, fibers, hydrogels and films and therefore with sizes in the range of approximately 100–150 μm for fibers diameters to the millimetric sizes of crystals [20,21,34–37]. In these microstructures, the residual of hydration layers and buffer solutions remains an uncontrolled parameter, affecting the final spectroscopic response. Measurements of DNA in solution are often performed at high concentration (up to 25 mg/ml). Such solution conditions can contribute to the aggregation of the biomolecules and can contribute to undesired interactions between different helices [34]. Several differences are introduced by the presence of the background caused by the solvent and the physical state of the DNA sample. Raman studies on DNA are frequently performed in highly hydrated states, but several work describe Raman Spectroscopy on solid samples [38–41]. All these parameters impact the spectral signature of the DNA sample, creating significant variability in the spectral signatures reported in previous literature. Our preparation method prevents all these uncontrollable environmental spectral and structural results.

Due to these limitations, there is an urgent need to develop new methodologies for evaluating the structural effects of a therapeutic dose of cisplatin on nucleic acids from patients. Nowadays, the advances in micro- and nanofabrication as well as the improved sensitivity of photodetectors open a new frontier of investigations on nanoscopic 1-D samples, extending, in the field of structural biology, the investigation to samples closer to their native dimension, as electrospun DNA fibers of diameters of an average diameter as low as 35 nm, reported by Maleckis and Denis [42]. In this context, super-hydrophobic substrates (SHS) can be employed to establish an innovative sample preparation procedure, efficient in terms of sample concentration, down to 1 fM, purity and of a reduced time for sample preparation [43]. In the case of DNA, micropatterned substrates are able to concentrate the sample in the form of nanometric filaments, suspended and free standing on the patterned surface [44]. Indeed, during the drying process, non-interacting compounds are removed from the DNA filaments [45]. This method allows the retention of the structural, spectral, and physical features of the native biomolecule, while avoiding contamination with the buffering solution, as proved by previous studies [44–46]. Also, the suspended filaments obtained in the dehydration process have diameters ranging from 8 to 150 nm [47] while their length is of approximately 12 μm, consistent with the 50 kbases sequence of the DNA strand. The nanoscale dimensionality allows studying a reduced number of molecules, thus avoiding the contribution of inter-helical interactions typically occurring in crystal samples and preventing the formation of undesired non-physiological structures [34]. Filaments formation on SHS allows controlling their dimension and orientation. Due to the reduced dimensions of the suspended filament, the interaction of few molecules at a time can be investigated by multiple techniques, such as Laser Doppler Vibrometry [46,47], Atomic Force Microscopy [48], Electron Microscopy [49], and microRaman spectroscopy [50].

In this work, filaments entirely made of DNA and ligands were investigated by microRaman spectral analysis, which is a sensitive technique able to provide detailed information on the chemical and

structural alteration of long DNA molecules in the range of 50 kilobases [51] upon environmental stress (i.e. covalent binding of drugs) at sub molecular level. To this end, we combined superhydrophobic substrates, to suspend biomolecules on a background free platform and confocal microRaman spectroscopy to achieve local structural information on the interaction between cisplatin and double strand nucleic acids, at low DNA concentrations (~30 nM) and by using long DNA molecules (~50 k bases). To further confirm and verify the formation of cisplatin-DNA crosslinks, direct imaging by HRTEM was performed on the suspended DNA samples after drug administration.

## 2. Experimental

### 2.1. Super-hydrophobic surfaces fabrication

Super-hydrophobic samples of micropillar arrays were obtained following the procedure reported in previous works [52]. Briefly, Silicon ⟨100⟩ wafers were used as a substrate [53] and a circular pattern of disks was realized by optical lithography within a layer of positive photoresist, while metals were deposited by a sputter coating. The metals deposited were, in this order: a 10 nm layer of Ti to promote adhesion of gold on Si, followed by a 50 nm Au layer, which is protected by 50 nm of Cr. Pillars of an approximate height of 10 μm were obtained by etching in a DRIE system, then the Cr layer was removed with a selective wet etching. The sample was first covered with a 1-nm-thick layer of $Al_2O_3$, deposited by means of atomic layer deposition, and then functionalized with perfluorodecyltrichlorosilane (FDTS) in a Molecular Vapor Deposition System to enhance the super-hydrophobic features of the device. Substrates for HRTEM were fabricated similarly: the holes and the pillars were defined by two different lithographic steps and subsequently etched with two different Deep reactive ion etching processes [54].

### 2.2. DNA solution preparation and deposition

λ-DNA (48.5 kbp, New England Biolabs, Ipswich, MA, USA) was preheated 10 min at 65 °C before the incubation with a saturating amount of CisPt (Alfa Aesar, Karlsruhe, Germany), as previously assessed by the titration curve reported in [47]. The samples were incubated for 72 h at 37 °C [47] in aqueous solution. CisPt-DNA complex was diluted in saline buffer solution (6.5 mM NaCl, 10 mM Tris HCl, pH 9.3), reaching the final concentration of 1 ng/μl before use [49]. A 5 μl droplet of the final solution was then pipetted on the SHS and placed on a hot plate to keep a ΔT of 5 °C between the sample and the environment [55,56]. The same volume of the sample has been drop casted on $CaF_2$ windows as negative control and for preliminary screening. The same samples were analyzed by Circular dichroism with a Jasco J-815 photometer. CD spectra were obtained by working at a scanning speed of 100 nm/min, a DIT of 4 s, a bandwidth of 1 nm and by accumulating 10 spectra.

### 2.3. Characterization of suspended samples

#### 2.3.1. Electron microscopy

The samples were imaged by Quanta 200 SEM (ThermoFisher Scientific, Waltham, US), working at an acceleration voltage of 3 kV and 25pA (substrates without holes) or 5 kV and at 43 pA of current (substrates with holes). HRTEM imaging was performed by using an aberration-corrected X-FEG Titan 60–300 TEM (ThermoFisher Scientific, Waltham, US) working at 80 keV and a Gatan Tridiem 865 image filter (GIF). The typical electron dose setting used for HRTEM imaging was about 10–20 electrons $Å^{-2}$/s, and the exposure time of the CCD camera of 0.3–1 s [57]. The obtained HRTEM images were then analyzed with Gatan software. The interbases distances were measured by generating the image FFT followed by the application of a spot mask for each of the four features visible in the FFT and the generation of the Inverse FFT (Fig. 2).

#### 2.3.2. Raman spectroscopy

Raman spectroscopy characterization has been performed by a WITec confocal Raman system (α-Raman WITec GmbH, Ulm, Germany), working with a 100× Zeiss objective, with a grating of 600 g/mm, and equipped with a 100 μm core fiber and a Newtown CCD (Oxford Instruments, Abingdon, United Kingdom) thermoelectric cooled at −80 °C. A solid-state laser, 532 nm was used as the excitation line, working at a laser power of ~4 mW. Each measure was acquired with Control Five software (WiTec, GmbH, Ulm, Germany). As negative control, working buffer solutions were drop casted onto $CaF_2$ windows and the spectra acquired after the complete dehydration of the droplet. The samples analyzed were (i) cisplatin solution and (ii) cisplatin solution in working buffer on $CaF_2$ windows, (iii) suspended cisplatin-DNA adducts and (iv) suspended pristine DNA. The spectra of the suspended materials were obtained by accumulating 150 spectra, each with an exposure time of 3 s. Each spectra presented is obtained by the average result of at least 15 spectra acquired over 10 different suspended filaments. Spectra analysis has been carried out as previously reported [45]. The averaged spectra Briefly, Raman wavenumbers were individually re-centered by a Lorentzian fit on a reference peak (521 $cm^{-1}$ for Silicon and 321 $cm^{-1}$ for $CaF_2$) and subtracted by the background in the spectral region 200–3900 $cm^{-1}$ [58]; the Gaussian broad peaks ascribed to water residuals in the region 2600–3800 $cm^{-1}$ have been excluded from the background calculation. The spectral contribution of each peak emerging from the noise level was defined by fitting a set of Lorentzian curves in the background-subtracted data, while peaks with amplitude comparable with the noise level and with full width at half maximum (FWHM) $< 2$ $cm^{-1}$ were not considered for further analysis. Large bands were fitted as a group of overlapping peaks. The number of peaks in each band was defined in order to maximize the $R^2$ adjusted parameter for each fit. For the evaluation of CisPt linkage to the DNA bases, spectra were normalized after background removal to the intensity of the peak centered at 1610 $cm^{-1}$ while the suspended samples were normalized to the intensity of the peak falling in the range 1460–1470 $cm^{-1}$ [59]. The region 900–1020 $cm^{-1}$ has been neglected in data analysis to avoid misleading assignments due to the contribution of the Silicon secondary peak.

## 3. Results and discussion

The discussion of the results in this section is related firstly to a preliminary verification of the cisplatin binding to the DNA double helix through Circular Dichroism (CD). The CD spectra of pristine and platinated DNA are reported in Fig. S1 (Supporting Information). The administration of cisplatin at saturating conditions [47] slightly affects the CD spectra of pristine DNA and the variations observed are strongly dependent on the adducts formation. We should point out that in this work we used concentration at the limit of the detection of the CD technique to make them complementary with spectroscopic and HRTEM data which on the other hand show remarkable variations, demonstrating the enhanced capability of our approach. DNA-Cisplatin CD spectra show an increase in dichroic signal of the positive band located around 273 nm [60] and a blue shift; the dichroic signal of the negative band around 245 nm is slightly reduced while the positive band around 220 nm shows a more appreciable decrease in dichroic signal (Supplementary Fig. 1). Therefore, despite the slight differences between the CD spectra they are in agreement with previously published literature assessing that those changes are markers of a conformational transition between A and B forms [61].

The bundle suspension over SHS has been verified through SEM while the structural effects of the cisplatin-DNA adduct formation has been detailed by HRTEM direct imaging (Section 3.1). Finally, the analysis of Raman spectra (Section 3.2) allowed obtaining structural and chemical information on the modification caused by the formation of the

covalent bond between the chemotherapy intercalant and the DNA.

### 3.1. Filaments suspension and adducts validation by electron microscopy

The assessment of biomolecules suspension on SHS and the integration of the cisplatin molecule into the double helix has been preliminary provided through scanning electron microscopy (SEM) and HRTEM, respectively.

The dehydration of the droplet deposited over the SHS allows the suspension of free-standing cisplatin-DNA fibers. The filaments are autonomously oriented (Fig. 1) and intrinsically ordered, as assessed by previously published experimental evidence [54] and in silico simulations [47,49,52,62]. A droplet residual of approximately 450 μm of non-suspended materials and buffering agents is visible in Fig. 1 panel a, and is surrounded by cisplatin-DNA fibers of diameters ranging from 70 nm down to a few nm while moving towards the most peripherical area of the device. They are visible as fainted lines and highlighted by arrows in Fig. 1 panels c,d. Additional SEM images are reported in Supplementary Fig. 2.

A filament of approximately 20 nm has been directly imaged through HRTEM revealing periodic arrangements related to interbases distances (Fig. 2). To identify and measure the spacing between bases from HRTEM images (Fig. 2, panel a top image), Discrete Fourier Transform (DFT) was applied (Fig. 2, bottom image of panel a), giving four main spots. An image representing the localization of each set of spatial frequencies is obtained through the inverse discrete Fourier transform (Fig. S3, Supporting Information) after proper masking, and used to extract the spatial frequency information from the acquired image. The resulting intensity profiles are reported in Fig. 2, panel b, and describe the periodic features of the image in the direct space. The Inverse DFT shows a path overlapping the HRTEM direct image and clearly identifies a spatial distribution of different interbases distance. The line profiling of the Inverse FFT obtained is reported in Supplementary Fig. 3. In the suspended sample it is possible to distinguish between four different periodicities, ascribed to three main DNA structural conditions. Firstly, an interbase distance of 5.6 Å is related to DNA denaturation caused by the interaction with cisplatin (as previously reported in [47]), a distance of 3.3 Å corresponds to the DNA double helix in the hydrated form while the distances of 2.8 and 2.2 Å are related to DNA in the most dehydrated form [37,49,63,64]. The DNA filament is composed of concentric layers of aligned DNA double helices which retain an inter-helical hydration layer of water for structural stability, justifying the presence of features related to DNA hydrated B-form [62] while the outer shell retain less water molecules. The bundle conformation composed of multiple aligned DNA double helices, allows the concurrent presence of different interbases distances in the same area.

### 3.2. Raman spectroscopy: Characterization of the cisplatin-DNA interaction

To assess the cisplatin fingerprint, the spectral analysis of the chemotherapeutic solution was evaluated on $CaF_2$ windows. The spectra study reveals the presence of two main peaks at 1610 $cm^{-1}$ and 1730 $cm^{-1}$ (Fig. 3, panel b) assigned to cisplatin $NH_3$ in plane deformation [65] and its presence is the spctral confirmation of the drug integration into the double helix. The same peaks are detected in the working buffer added of cisplatin, along with Tris-HCl characteristic main bands in the spectral region 600–1800 $cm^{-1}$ at 760, 1064, and 1467 $cm^{-1}$ [66]. In

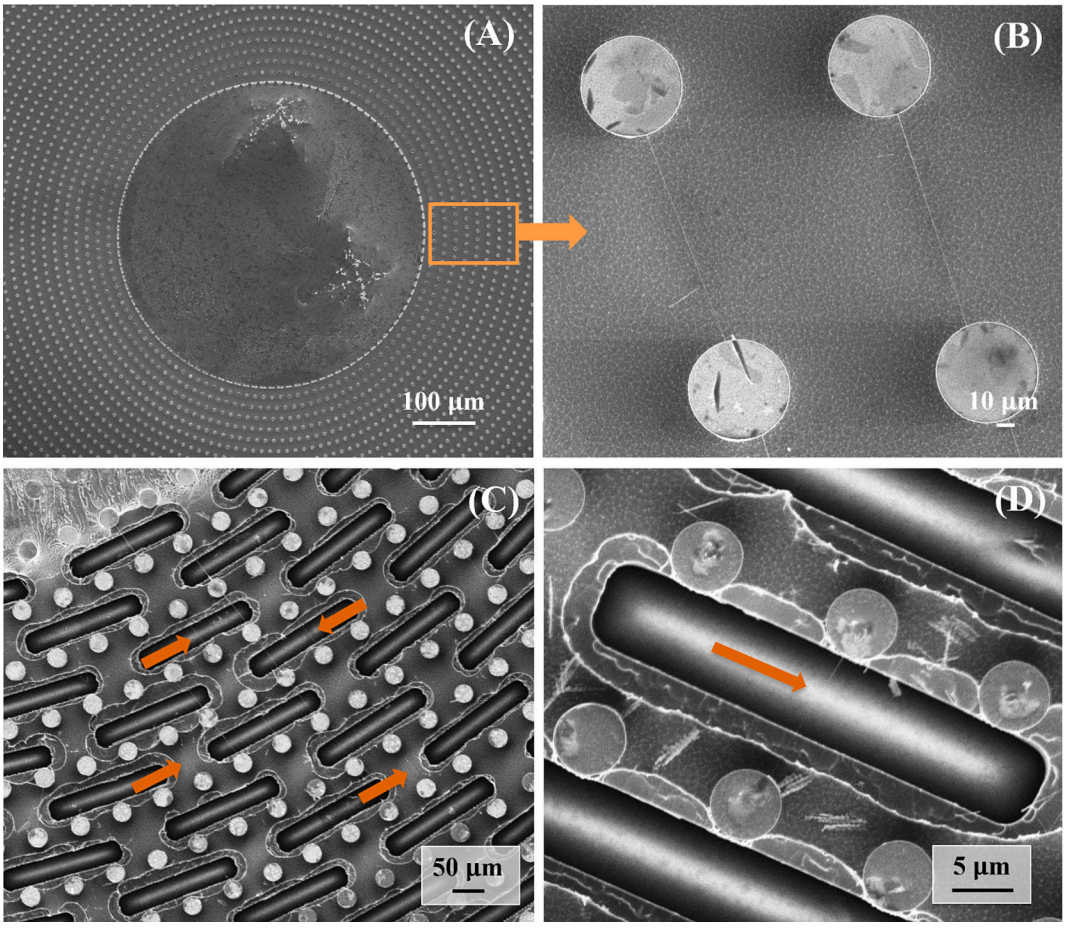


**Fig. 1.** SEM micrographs of circularly patterned SHS; a) low magnification picture of the drying residual b) DNA bundles suspended between two couples of pillars; c, d) DNA bundles suspended on top of the holes, which allow TEM imaging. Arrows indicate the presence of suspended DNA bundles on top of the holes.

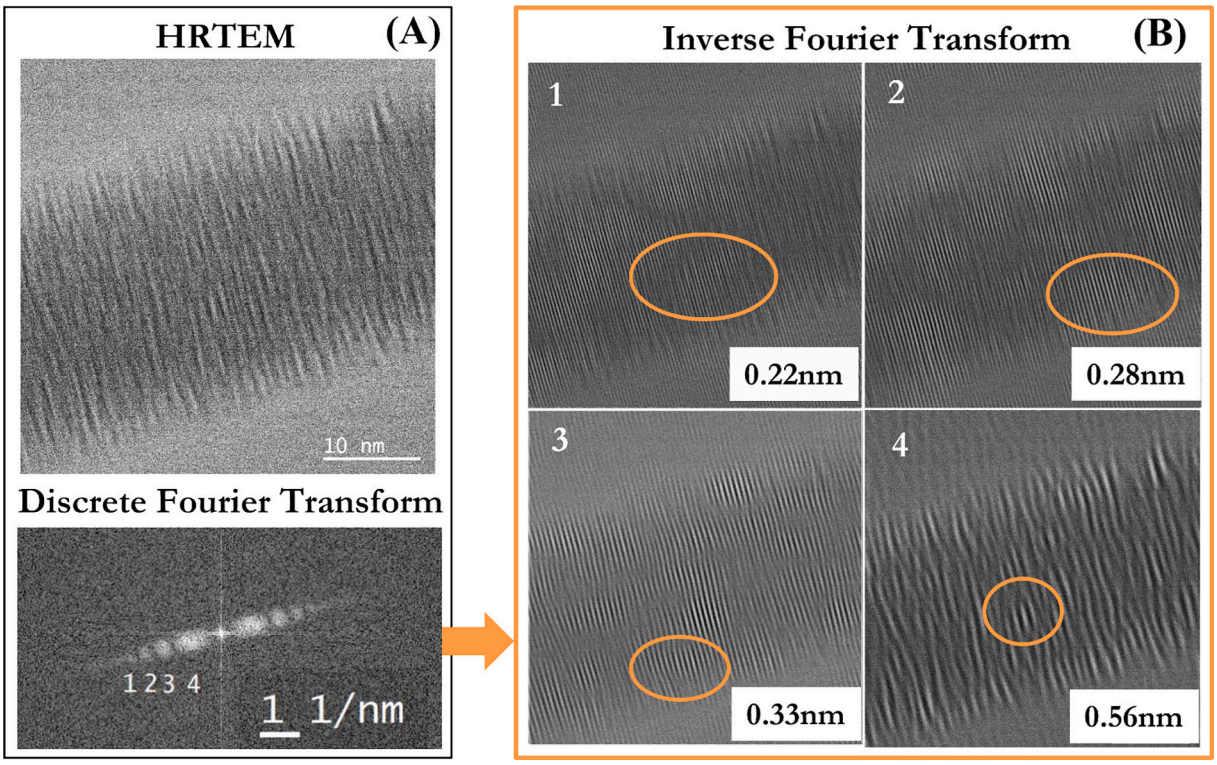


**Fig. 2.** (a) HRTEM of a 20 nm bundle of a cisplatin-DNA and the related Discrete Fourier Transform. (b) The Inverse Fourier Transform obtained by the analysis of the cisplatin-DNA adduct of the HRTEM image describes the simultaneous presence of different DNA interbase distances, related to less (0.22, 0.28 nm) or more hydrated double helices (0.33 nm) along with local DNA denaturation (0.56 nm).

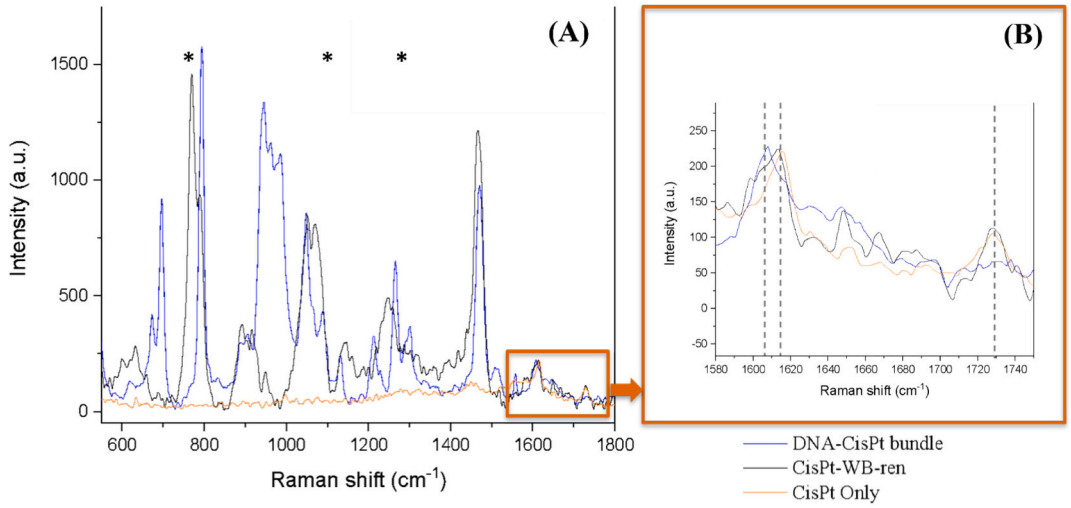


**Fig. 3.** Normalized Raman spectra of cisplatin aqueous solution, of cisplatin in a Tris-based buffer, and of a cisplatin-DNA suspended filament, showing the presence of the *chemotherapeutic* drug in all the samples reported. The spectra shown are normalized to the peak centered around 1610 cm$^{-1}$ and related to cisplatin. (a) The buffer spectra show prominent peaks of the Tris cation (highlighted by asterisks and labels) with the characteristic main bands at 760, 1064, and 1467 cm$^{-1}$ [66]. (b) The peak centered around 1730 cm$^{-1}$ is present only when cisplatin is dissolved in solution and is not detected after its interaction with DNA. A shift in the band.

the region 2500–3750 cm$^{-1}$, Tris-related bands are centered around 3292 cm$^{-1}$ and 3350 cm$^{-1}$ (Fig. 4, Supporting Information) while no contribution from cisplatin is detected.

In our experimental conditions, the suspended sample is obtained from a starting solution composed by the cisplatin-DNA complex, monovalent cations ($Na^+$) and Tris-HCl buffering agent (Fig. 3, panels a, b). The spectra show the characteristic signature of the vibrations related to the DNA phosphate group, the deoxyribonucleic sugar, the bases [28] and Cisplatin [67]. It has to be noted that the spectra of the suspended cisplatin-DNA filaments are free from any contribution from Tris-related signature. In fact, during the dehydration process on SHS substrates, Tris cation are autonomously sieved out from the filaments, removing the non-interacted cations from the areas of investigation, as discussed in previous literature [45]. The suspended sample therefore is free from any additional signature contributions from the buffer which, in solution or deposited on flat substrates, overwrites most of the Raman features from the molecule.

With this premise, Raman peaks provide spectral information free

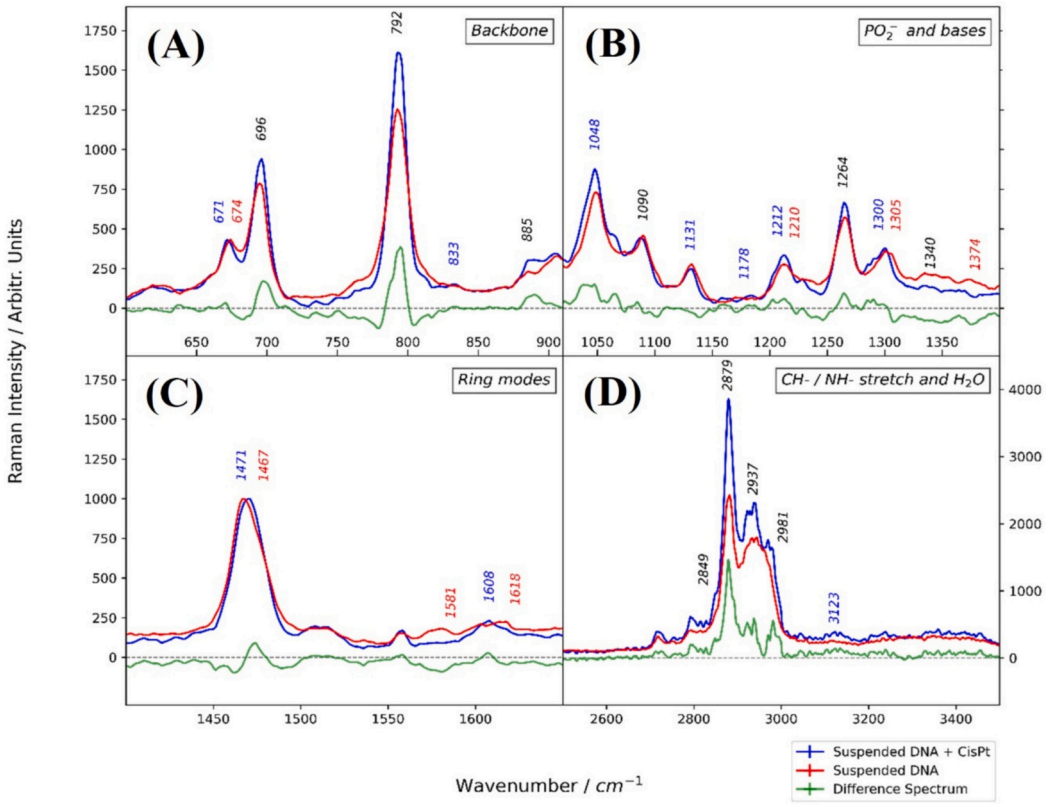


**Fig. 4.** Raman spectra of suspended cisplatin-DNA filaments (blue), free-standing pristine DNA (red), and their computed difference (green) in the range 600–920 $cm^{-1}$ in panel a), 1020–1400 $cm^{-1}$ in panel b), 1400–1750 $cm^{-1}$ in panel c), and 2500–3750 $cm^{-1}$ in panel d). The Raman spectra were normalized to a peak at 1468 $cm^{-1}$ assigned to the 5'$CH_2$ scissor mode [45]. Peaks common to both spectra are labeled in black. Peaks labeled in blue and red correspond to suspended cisplatin-DNA and pristine DNA, respectively. The main spectral differences in terms of wavenumbers are reported as label on the graph. (For interpretation of the references to colour in this figure legend, the reader is referred to the web version of this article.)

from buffer excess, allowing the analysis only of the dry DNA filaments and the materials effectively interacting with the nucleotides.

### 3.3. Raman spectroscopy: Characterization of the cisplatin-DNA complex

The alterations of the DNA structure occurring upon the interaction with the chemotherapeutic compound were studied through the difference spectra (green line, Fig. 4 and Supporting Fig. 5) between the signature of the filaments treated with cisplatin and the suspended pristine DNA fingerprint after the renormalization to a reference peak (refer to Materials and Methods section). The deviation standard is indicated in supplementary Fig. 6 along with the averaged spectra. The spectral region 600–1650 $cm^{-1}$ (Fig. 4a) showed details on the double helix form, sugar and bases conformation, and the phosphate backbone while the range 2500–3750 $cm^{-1}$ (Fig. 4d) is related to the deoxyribosyl CH stretching vibrations and water contributions. The peak centered around 1610 $cm^{-1}$ is assigned to cisplatin and its presence is the spectral confirmation of the drug integration into the double helix. To analyze the effects of cisplatin covalent binding in the DNA double helix a preliminary description of the spectral signatures of pristine suspended DNA filaments is provided, followed by the comparison with spectral information from cisplatin-DNA suspended filaments. In Table 1 are reported the main variations in Raman wavenumbers of the two compared samples and the related assignments.

#### 3.3.1. Pristine suspended DNA

The peaks centered at 674 $cm^{-1}$ and around 680 $cm^{-1}$ are indicative of a $C_2'$-endo and a $C_3'$-endo conformation, respectively [20,21], and are related to the ring mode of guanine, used for the identification of DNA conformation. In this case the peaks identify DNA in the A and B-form, respectively. The suspended filament of DNA is composed of double helices arranged in concentrical layers [62]. The outer layers exposed to the environment previously showed features compatible with the A-DNA form [49] while the inner layers of the suspended material retain a 0.3 nm solvation layer [62]. The presence of different hydration levels of the filament are therefore reflected into the conformational details of the biomolecules studies [44].

The range 790–840 $cm^{-1}$ describes the phosphate backbone stretching mode and allows distinguishing between different conformers of DNA. In our case, the bands centered at 792 $cm^{-1}$ and the broad band at 834 $cm^{-1}$ are related to B-DNA and can be compared to those reported for cisplatin-DNA adducts [22]. The two neighboring Raman bands at 788 $cm^{-1}$ and 807 $cm^{-1}$ are visible as shoulders of the main peak at 792 $cm^{-1}$. Despite the weak contribution, these bands are associated to the A-form of DNA as reported in previous literature related to DNA in hydrated gels or fibers [20]. Also, Lindsay et al. [34], demonstrated the decrease of the intensity of 807 $cm^{-1}$ marker while diminishing the relative humidity. Deoxyribose vibrations are related to the presence of two bands at 896 $cm^{-1}$ and 1047 $cm^{-1}$ and related to deoxyribose and to C—O stretching [68].

The $PO_2^-$ stretching mode in suspended pristine DNA samples is centered at 1090 $cm^{-1}$ and is related to B-DNA [41,69,70], corroborated by the presence of the 834 $cm^{-1}$ B-DNA marker band. The phosphodioxy vibration is also present at 1102 $cm^{-1}$ and is diagnostic of an A-DNA vibration [71] of the outer layer of dehydrated DNA.

The vibrations related to the bases can be observed in the range 1100 $cm^{-1}$–1700 $cm^{-1}$. This range is informative about base pairing, as it depends on the electronic properties of the base residues. In our case, the most intense bands are assigned to (i) adenine, at 1210 $cm^{-1}$, 1305 $cm^{-1}$, 1343 $cm^{-1}$, and 1581 $cm^{-1}$ [72] (ii) cytosine at 1264 $cm^{-1}$ [20],

**Table 1**
This table reports on the main variations in Raman wavenumbers of suspended cisplatin-DNA with respect to pristine DNA suspended filaments taken as a reference. The assignments reported in the table refer to the four nucleotides (bases+sugar) adenine, thymine, guanine, and cytosine, A- and B-DNA conformers (A-DNA and B-DNA), phosphate ($PO_2^-$) group of the backbone, the deoxyribose sugar of the DNA backbone. sh, shoulder; vs, very strong; s, strong; m, medium; w, weak; vw very weak.

| Cisplatin-DNA | Pristine DNA | Assignment |
|---|---|---|
| Wavenumber ($cm^{-1}$) | Wavenumber ($cm^{-1}$) | |
| 671 | 674 | Guanine ring breathing (A-DNA) [28] |
| 780 | 780 (w) | Cytosine ring breathing [82] |
| 792 (vs) | 792 (s) | O—P—O single bond stretching vibration (B-DNA) [35] |
| – | 804 | Phosphate backbone main chain A-form [82] |
| 834 (m) | – | Phosphate backbone main chain B-form [21] |
| 885 | 885 | Backbone deoxyribose [68] |
| 902 | 902 | Backbone deoxyribose [83] |
| 930–1020 | 930–1020 | Silicon secondary peak |
| 1048 (vs) | 1048 (s) | Backbone deoxyribose (vCO) [68] |
| 1066 (sh) | – | Backbone symmetric CO stretching [83] |
| 1088 | 1091 | $PO_2^-$ symmetric stretching [69] |
| – | 1102 | A helix $PO_2^-$ [36] |
| – | 1138 | |
| 1131 | 1132 | C—C stretching [20] |
| 1178 | – | Unpaired thymine [76] |
| 1203 | – | Thymine, Adenine [79] |
| 1212 | 1212 | Thymine, Adenine [76] |
| – | 1223 | $PO_2^-$ asymmetric vibration [69] |
| – | 1236 | Thymine, Cytosine [66] |
| – | 1246 | $PO_2^-$ asymmetric vibration [73] |
| 1265 (vs) | 1265 (s) | Cytosine [84] |
| 1286 | – | Cytosine [85] |
| 1290 | – | C—C stretching |
| 1300 | 1300 | Adenine N7═C8 [75] |
| | 1308 | Adenine |
| 1340 | 1340 | Adenine, guanine C5—N7 [75] |
| – | 1376 | Thymine-Major groove marker peak [86] |
| 1471 | 1467 | Guanine [87] |
| 1608 | – | Cisplatin [65] |
| 1618 | – | GC carbonyl stretching [23] |
| 2849 | 2849 | |
| 2879 | 2879 | deoxyribosyl CH stretching vibrations |
| 2937 | 2937 | [20] |
| 2981 | 2981 | |
| 3123 | – | guanine C8—H stretching [80] |
| 3237 | 3237 | Water |
| 3400 | 3400 | |

(iii) thymine at 1210 $cm^{-1}$, 1374 $cm^{-1}$ and (iv) guanine at 1464 $cm^{-1}$, 1343 $cm^{-1}$ and 1581 $cm^{-1}$ [36]. The contribution of adenine and guanine overlaps at 1343 $cm^{-1}$ and 1581 $cm^{-1}$ [36]. The bands centered at 1223 and 1245 $cm^{-1}$ are related to the $PO_2^-$ asymmetric stretch vibration in pristine DNA [73].

The Raman large band centered around 1340 $cm^{-1}$ is sensitive to adenine conformation and to the rearrangement of H-bonds at the acceptor site N7 of adenine. This band is split into two different peaks due to the mechanical coupling of the base with the sugar moiety: the peak at 1344 $cm^{-1}$ indicates the presence of the $C_2'$-endo conformation, while the lower peak at 1332 $cm^{-1}$ is associated with a less frequent $O_4'$-endo sugar pucker [72].

### 3.3.2. *Cisplatin-DNA suspended filaments*

Platination affects the nucleic acids spectra, and the predominant changes are observed for the backbone vibration, ring breathing, and stretching modes of adenine, guanine and thymine. The frequency at 671 $cm^{-1}$ is characteristic of a $C_2$'-endo conformational isomer [20,21] and corresponds to a slightly red-shift with respect to pristine DNA (671 $cm^{-1}$ from 674 $cm^{-1}$). The OPO single bond symmetric and asymmetric stretching vibrations are related to the band centered at 792 $cm^{-1}$ and the broad band at 834 $cm^{-1}$ and define a deoxyribose-phosphate main chain of a B-DNA conformer [35,74]. Both contributions are more intense in platinated DNA with respect to pristine DNA.

The phosphodioxy marker band ($PO_2^-$) in the suspended cisplatin-DNA sample is downshifted of 4 $cm^{-1}$ (from 1091 to 1087 $cm^{-1}$) with respect to the suspended pristine DNA and indicates a relaxation of the double helix structure in accordance with previous literature [20]; this effect is supported also by the suppression of the phosphodioxy vibration at 1102 $cm^{-1}$ (A-DNA), present only in suspended native DNA samples [71]. The bands related to the $PO_2^-$ asymmetric stretch vibrations, present in pristine DNA are blocked under platination conditions [73].

The peaks at 1210 $cm^{-1}$, 1300 $cm^{-1}$ and 1338 $cm^{-1}$ correspond respectively to the adenine and thymine ring modes, to the coupled stretching vibrations of N7═C8, and to C5—N7 stretching localized on the purine ring of adenine [75]. The peak at 1210 $cm^{-1}$ is slightly shifted to 1212 $cm^{-1}$ and it is broadened towards 1204 $cm^{-1}$, as evident from the difference spectrum (Fig. 4b). A slight increase in the intensity of the signal at 1182 $cm^{-1}$ is also detected. These combined findings assess the alteration of the A-T hydrogen bonding network with respect to pristine DNA. Also, similar assignments were previously described upon melting of A-T polynucleotides [76,77].

In the platinated sample, the whole band at 1340 $cm^{-1}$ is less intense with respect to pristine DNA but centered on the same frequency, whereas the shoulder at 1305 $cm^{-1}$ in pristine DNA it is red shifted to 1300 $cm^{-1}$. Moreover, it presents two shoulders, attributed to the superposition of guanine C5—N7 vibration, with the in-plane and out-of-plane $NH_3$ cisplatin deformation found in cisplatin-adenine crosslinks [65]. The 1374 $cm^{-1}$ band, attributed to the $CH_3$ deformation in adenine, thymine, and guanine, is less intense in the drug treated sample while is present in the pristine DNA sample; a similar behavior has been reported for cisplatin binding to salmon sperm DNA [23,76,77]. The guanine band at 1471 $cm^{-1}$ is blue shifted (4 $cm^{-1}$) while the peak at 1581 $cm^{-1}$ is absent with respect to pristine DNA. These assignments are consistent with previously reported literature on DNA platination studies [13]. At last, the cytosine peak at 1264 $cm^{-1}$ is more intense in the cisplatin treated sample. The peak intensity increase of the bands related to thymine and cytosine centered at 1212 and 1265 $cm^{-1}$, respectively, is in good agreement with previously reported in studies related to DNA melting and pre-melting transition and DNA packing and describes base unstacking [78,79].

Spectral differences between platinated and pristine DNA structures can also be detected in the region 2800–3000 $cm^{-1}$ (Fig. 4, panel b) and related to the deoxyribosyl CH stretching vibrations [20,78]. In DNA exposed to cisplatin, the bands centered at 2849 and 2879 $cm^{-1}$ showed higher intensity while the band between 2900 $cm^{-1}$ and 3000 $cm^{-1}$ is split into two contributions at 2937 $cm^{-1}$ and 2981 $cm^{-1}$ and associated to the less hydrated A-DNA conformer [20]. The band at 3123 $cm^{-1}$ can be assigned to guanine C—H stretching [80].

The previous assignments endorse the conclusion that, regarding DNA conformation, a transition to a loosen state of DNA can be assessed, particularly through the Raman marker peaks sensitive to DNA conformation as the 671 $cm^{-1}$ peak (guanine ring breathing), 792 $cm^{-1}$ and 834 $cm^{-1}$ peaks (phosphate backbone symmetric stretching), and the 1090, 1225, and 1245 $cm^{-1}$ peaks (symmetric and antisymmetric $PO_2^-$ vibrations). These findings are strongly supported by the HRTEM direct images acquired on the same samples. Moreover, ring vibrations are more intense in the platinated sample, suggesting the unstacking and an altered hydrogen bond network of the bases, as found in melting and pre-melting transitions [76,79,81]. Finally, it is confirmed that cisplatin binds preferentially to the guanine and adenine residues of DNA upon the formation of covalent bonds. Bands assigned to cytosine were not altered in terms of wavenumbers by drug administration, whereas the thymine-related bands were modified in both intensity and

wavenumbers [24,44].

## 4. Conclusions

It is well known that conformational transitions can occur in physiological conditions and depend upon hydration variations, solution and sequence composition [88,89] but can also reflect a non-physiological condition, precluding the correct functioning of the cellular machine [90–92]. In this work, we applied a quantitative method to unveil the integration mechanism of drugs into double helix and evaluate the structural effects of such modification to pristine DNA molecules. Data normalization allowed us to obtain a repeatable and quantitative analysis and directly comparing signals along the filament and between different filaments of the same device. Another key point in our study lies in the extended sampling of our analyte of interest: the presence of multiple filaments on the same device, arising from the same solution of analytes, led to uncovering fine variations in the structure of DNA upon cisplatin binding despite the small dimensions of the analyzed fibers. The genetic material did not need any purification or preliminary process to emerge from other interfering buffering agents or non-interacting molecules excesses. The simplified preparation strategy allows obtaining oriented filaments starting from biomaterials in solution in approximately 1 hour; sub molecular portions along the suspended filament have been co-localized and characterized by multiple techniques for a complete overview of the chemical and structural variations of the biosystem. The microRaman study on the DNA-SHS we proposed in this work demonstrated that the formation of cisplatin-DNA adducts causes helical distortion, detected with a conformational transition towards a more relaxed conformer of DNA and with the local denaturation of the double helix sequence. This evidence suggests that drug administration induces cytotoxicity through the alteration of DNA forms and consequently affecting transcription and replication. The case presented in this work relies on a well-known chemotherapeutic molecule such as cisplatin; we herein use a novel methodology to address biomedical questions and, to assess our method reliability. The promising results demonstrate how this approach is capable of showing how chemical modifications induce structural changes after drug administrations at sub molecular level. It is therefore a strong candidate platform to study the effects of unknown drugs.

## Ethics approval statement

No ethics approval was required for this work.

## Declaration of competing interest

The authors declare that they have no known competing financial interests or personal relationships that could have appeared to influence the work reported in this paper.

## Acknowledgements

This research has been co-funded by the European Union - Next Generation EU Program within the project SOE_0000167 Intramolecular DNA Structural Studies (InStruct) and by the Italian Ministry of Health within the “CAL.HUB.RIA” project.

## Appendix A. Supplementary data

Supplementary data to this article can be found online at https://doi.org/10.1016/j.saa.2025.126606.

## Data availability

Data will be made available through Zenodo repository.

## References

[1] Drugs@FDA: FDA-Approved Drugs, (n.d.). https://www.accessdata.fda.gov/scripts/cder/daf/index.cfm (accessed October 7, 2024).
[2] S. Ghosh, Cisplatin: the first metal based anticancer drug, Bioorg. Chem. 88 (2019) 102925, https://doi.org/10.1016/j.bioorg.2019.102925.
[3] M.A. Fuertes, J. Castilla, C. Alonso, J.M. Perez, Novel concepts in the development of platinum antitumor drugs, Curr. Med. Chem. - Anti-Cancer Agents 2 (2002) 539–551, https://doi.org/10.2174/1568011023353958.
[4] M.A. Fuertes, C. Alonso, J.M. Pérez, Biochemical modulation of cisplatin mechanisms of action: enhancement of antitumor activity and circumvention of drug resistance, Chem. Rev. 103 (2003) 645–662, https://doi.org/10.1021/cr020010d.
[5] A.M.J. Fichtinger-Schepman, J.L. Van Der Veer, J.H.J. Den Hartog, P.H. M. Lohman, J. Reedijk, Adducts of the antitumor drug cis-diamminedichloroplatinum(II) with DNA: formation, identification, and quantitation, Biochemistry 24 (1985) 707–713, https://doi.org/10.1021/bi00324a025.
[6] S. Mansy, G.Y.H. Chu, R.E. Duncan, R.S. Tobias, Heavy metal nucleotide interactions. 12. Competitive reactions in systems of four nucleotides with cis- or trans-diammineplatinum(II). Raman difference spectrophotometry of the relative nucleophilicity of guanosine, cytidine, adenosine, and uridine monophosphates and analogous DNA bases, J. Am. Chem. Soc. 100 (1978) 607–616, https://doi.org/10.1021/ja00470a040.
[7] C.A. Rabik, M.E. Dolan, Molecular mechanisms of resistance and toxicity associated with platinating agents, Cancer Treat. Rev. 33 (2007) 9–23, https://doi.org/10.1016/j.ctrv.2006.09.006.
[8] L. Kelland, The resurgence of platinum-based cancer chemotherapy, Nat. Rev. Cancer 7 (2007) 573–584, https://doi.org/10.1038/nrc2167.
[9] A. Vaisman, S.E. Lim, S.M. Patrick, W.C. Copeland, D.C. Hinkle, J.J. Turchi, S. G. Chaney, Effect of DNA polymerases and high mobility group protein 1 on the carrier ligand specificity for Translesion synthesis past platinum−DNA adducts, Biochemistry 38 (1999) 11026–11039, https://doi.org/10.1021/bi9909187.
[10] L. Astolfi, S. Ghiselli, V. Guaran, M. Chicca, E. Simoni, E. Olivetto, G. Lelli, A. Martini, Correlation of adverse effects of cisplatin administration in patients affected by solid tumours: a retrospective evaluation, Oncol. Rep. 29 (2013) 1285–1292, https://doi.org/10.3892/or.2013.2279.
[11] O. Bhatavdekar, I. Godet, D. Gilkes, S. Sofou, The rate of cisplatin dosing affects the resistance and metastatic potential of triple negative breast cancer cells, independent of hypoxia, Pharmaceutics 14 (2022) 2184, https://doi.org/10.3390/pharmaceutics14102184.
[12] E.R. Jamieson, S.J. Lippard, Structure, recognition, and processing of cisplatin-DNA adducts, Chem. Rev. 99 (1999) 2467–2498, https://doi.org/10.1021/cr980421n.
[13] O. Vrána, V. Mašek, V. Dražan, V. Brabec, Raman spectroscopy of DNA modified by intrastrand cross-links of antitumor cisplatin, J. Struct. Biol. 159 (2007) 1–8, https://doi.org/10.1016/j.jsb.2007.01.008.
[14] H. Ouzon-Shubeita, M. Baker, M.-C. Koag, S. Lee, Structural basis for the bypass of the major oxaliplatin-DNA adducts by human DNA polymerase η, Biochem. J. 476 (2019) 747–758, https://doi.org/10.1042/BCJ20180848.
[15] P.M. Takahara, A.C. Rosenzweig, C.A. Frederick, S.J. Lippard, Crystal structure of double-stranded DNA containing the major adduct of the anticancer drug cisplatin, Nature 377 (1995) 649–652, https://doi.org/10.1038/377649a0.
[16] B. Wu, G.E. Davey, A.A. Nazarov, P.J. Dyson, C.A. Davey, Specific DNA structural attributes modulate platinum anticancer drug site selection and cross-link generation, Nucleic Acids Res. 39 (2011) 8200–8212, https://doi.org/10.1093/nar/gkr491.
[17] R.C. Todd, S.J. Lippard, Structure of duplex DNA containing the cisplatin 1,2-{Pt(NH3)2}2+−d(GpG) cross-link at 1.77 Å resolution, J. Inorg. Biochem. 104 (2010) 902–908, https://doi.org/10.1016/j.jinorgbio.2010.04.005.
[18] H. Huang, L. Zhu, B.R. Reid, G.P. Drobny, P.B. Hopkins, Solution structure of a cisplatin-induced DNA Interstrand cross-link, Science 270 (1995) 1842–1845, https://doi.org/10.1126/science.270.5243.1842.
[19] J.-M. Teuben, C. Bauer, A.H.-J. Wang, J. Reedijk, Solution structure of a DNA duplex containing a *cis* -Diammineplatinum(II) 1,3-d(GTG) Intrastrand cross-link, a major adduct in cells treated with the anticancer drug carboplatin, Biochemistry 38 (1999) 12305–12312, https://doi.org/10.1021/bi9904757.
[20] B. Prescott, W. Steinmetz, G.J. Thomas, Characterization of DNA structures by laser Raman spectroscopy, Biopolymers 23 (1984) 235–256, https://doi.org/10.1002/bip.360230206.
[21] G.J. Thomas, J.M. Benevides, S.A. Overman, T. Ueda, K. Ushizawa, M. Saitoh, M. Tsuboi, Polarized Raman spectra of oriented fibers of a DNA and B DNA: anisotropic and isotropic local Raman tensors of base and backbone vibrations, Biophys. J. 68 (1995) 1073–1088, https://doi.org/10.1016/S0006-3495(95)80282-1.
[22] J.M. Benevides, S.A. Overman, G.J. Thomas Jr., Raman, polarized Raman and ultraviolet resonance Raman spectroscopy of nucleic acids and their complexes, J. Raman Spectrosc. 36 (2005) 279–299, https://doi.org/10.1002/jrs.1324.
[23] A.J.P. Alix, L. Bernard, M. Manfait, P.K. Ganguli, T. Theophanides, Binding of *cis*- and *trans*-dichlorodiammineplatinum(II) to nucleic acids studied by Raman spectroscopy. Part. I. Salmon sperm DNA, Inorg. Chim. Acta 55 (1981) 147–152, https://doi.org/10.1016/S0020-1693(00)90797-7.
[24] J. Geng, M. Aioub, M.A. El-Sayed, B.A. Barry, An ultraviolet resonance Raman spectroscopic study of cisplatin and Transplatin interactions with genomic DNA, J. Phys. Chem. B 121 (2017) 8975–8983, https://doi.org/10.1021/acs.jpcb.7b08156.

[25] A.M. Tamburro, V. Guantieri, Conformation of poly(dG-dC)·poly(dG-dC) and poly (dA-dT)·poly(dA-dT) interacting with the antitumor drug cis-[Pt(NH32]Cl2, Inorg. Chim. Acta 92 (1984) 229–233, https://doi.org/10.1016/S0020-1693(00)87763-4.
[26] A. Barhoumi, D. Zhang, F. Tam, N.J. Halas, Surface-enhanced Raman spectroscopy of DNA, J. Am. Chem. Soc. 130 (2008) 5523–5529, https://doi.org/10.1021/ja800023j.
[27] B. Giese, D. McNaughton, Interaction of anticancer drug cisplatin with guanine: density functional theory and surface-enhanced Raman spectroscopy study, Biopolymers 72 (2003) 472–489, https://doi.org/10.1002/bip.10480.
[28] W. Safar, A. Azziz, M. Edely, M. Lamy de la Chapelle, Conventional Raman, SERS and TERS studies of DNA compounds, Chemosensors 11 (2023) 399, https://doi.org/10.3390/chemosensors11070399.
[29] I. Bianchi-Carvalho, M.J.D.S. Oliveira, C.S. Martin, S. Sánchez-Cortés, C.J. L. Constantino, Influence of sample preparation on SERS signal, Chemosensors 13 (2025) 22, https://doi.org/10.3390/chemosensors13010022.
[30] D.K. Jangir, R. Mehrotra, Raman spectroscopic evaluation of DNA adducts of a platinum containing anticancer drug, Spectrochim. Acta A Mol. Biomol. Spectrosc. 130 (2014) 386–389, https://doi.org/10.1016/j.saa.2014.04.030.
[31] T. Kishimoto, Y. Yoshikawa, K. Yoshikawa, S. Komeda, Different effects of cisplatin and Transplatin on the higher-order structure of DNA and gene expression, Int. J. Mol. Sci. 21 (2020) 34, https://doi.org/10.3390/ijms21010034.
[32] T. O'Connor, S. Mansy, M. Bina, D.R. McMillin, M.A. Bruck, R.S. Tobias, The pH-dependent structure of calf thymus DNA studied by Raman spectroscopy, Biophys. Chem. 15 (1982) 53–64, https://doi.org/10.1016/0301-4622(82)87016-6.
[33] M. Gąsior-Głogowska, K. Malek, G. Zajac, M. Baranska, A new insight into the interaction of cisplatin with DNA: ROA spectroscopic studies on the therapeutic effect of the drug, Analyst 141 (2015) 291–296, https://doi.org/10.1039/C5AN02140E.
[34] S.M. Lindsay, S.A. Lee, J.W. Powell, T. Weidlich, C. Demarco, G.D. Lewen, N. J. Tao, A. Rupprecht, The origin of the a to B transition in DNA fibers and films, Biopolymers 27 (1988) 1015–1043, https://doi.org/10.1002/bip.360270610.
[35] S.C. Erfurth, P.J. Bond, W.L. Peticolas, Characterization of the a ⇄ B transition of DNA in fibers and gels by laser Raman spectroscopy, Biopolymers 14 (1975) 1245–1257, https://doi.org/10.1002/bip.1975.360140613.
[36] J.M. Benevides, A.H.J. Wang, A. Rich, Y. Kyogoku, G.A. Van Der Marel, J.H. Van Boom, G.J. Thomas, Raman spectra of single crystals of r(GCG)d(CGC) and d (CCCCGGGG) as models for a DNA, their structure transitions in aqueous solution, and comparison with double-helical poly(dG).Cntdot.Poly(dC), Biochemistry 25 (1986) 41–50, https://doi.org/10.1021/bi00349a007.
[37] R.E. Franklin, R.G. Gosling, Molecular configuration in sodium Thymonucleate, Nature 171 (1953) 740–741, https://doi.org/10.1038/171740a0.
[38] V.S. Gorelik, A.S. Krylov, V.P. Sverbil, Local Raman spectroscopy of DNA, Bull. Lebedev Phys. Inst. 41 (2014) 310–315, https://doi.org/10.3103/S1068335614110025.
[39] B.S. Kalanoor, M. Ronen, Z. Oren, D. Gerber, Y.R. Tischler, New method to study the vibrational modes of biomolecules in the terahertz range based on a single-stage Raman spectrometer, ACS Omega 2 (2017) 1232–1240, https://doi.org/10.1021/acsomega.6b00547.
[40] A.Yu. Sosorev, O.D. Paraschuk, A.A. Trubitsyn, N.O. Dubinets, I.V. Chicherin, D. Yu. Paraschuk, Assessment of dynamic disorder in DNA oligonucleotides using low-frequency Raman spectroscopy, Moscow Univ. Phys. 79 (2024) 248–258, https://doi.org/10.3103/S002713492470019X.
[41] A. Japaridze, D. Vobornik, E. Lipiec, A. Cerreta, J. Szczerbinski, R. Zenobi, G. Dietler, Toward an effective control of DNA'S submolecular conformation on a surface, Macromolecules 49 (2016) 643–652, https://doi.org/10.1021/acs.macromol.5b01827.
[42] K. Maleckis, Y. Dzenis, Continuous DNA nanofibers with extraordinary mechanical properties and high molecular orientation, Macromol. Mater. Eng. 303 (2018) 1800302, https://doi.org/10.1002/mame.201800302.
[43] F. De Angelis, F. Gentile, F. Mecarini, G. Das, M. Moretti, P. Candeloro, M. L. Coluccio, G. Cojoc, A. Accardo, C. Liberale, R.P. Zaccaria, G. Perozziello, L. Tirinato, A. Toma, G. Cuda, R. Cingolani, E. Di Fabrizio, Breaking the diffusion limit with super-hydrophobic delivery of molecules to plasmonic nanofocusing SERS structures, Nat. Photon 5 (2011) 682–687, https://doi.org/10.1038/nphoton.2011.222.
[44] M. Marini, M. Allione, B. Torre, M. Moretti, T. Limongi, L. Tirinato, A. Giugni, G. Das, E. di Fabrizio, Raman on suspended DNA: novel super-hydrophobic approach for structural studies, Microelectron. Eng. 175 (2017) 38–42, https://doi.org/10.1016/j.mee.2016.12.016.
[45] M. Marini, B. Torre, M. Allione, T. Limongi, F. Legittimo, A. Giugni, C. Ricciardi, C. F. Pirri, E. di Fabrizio, Self-sieving DNA over superhydrophobic surfaces: a Raman spectroscopy study, J. Raman Spectrosc. 53 (2022) 1352–1360, https://doi.org/10.1002/jrs.6368.
[46] F. Legittimo, M. Marini, S. Stassi, E. Di Fabrizio, C. Ricciardi, Real-time monitoring of temperature-dependent structural transitions in DNA Nanomechanical resonators: unveiling the DNA–ligand interactions for biomedical applications, ACS Appl. Nano Mater. 6 (2023) 2249–2257, https://doi.org/10.1021/acsanm.2c05601.
[47] S. Stassi, M. Marini, M. Allione, S. Lopatin, D. Marson, E. Laurini, S. Pricl, C.F. Pirri, C. Ricciardi, E. Di Fabrizio, Nanomechanical DNA resonators for sensing and structural analysis of DNA-ligand complexes, Nat. Commun. 10 (2019) 1690, https://doi.org/10.1038/s41467-019-09612-0.
[48] F. Legittimo, M. Marini, S. Stassi, M. Tortello, J. Sader, P. Ashby, B. Rad, C. Ralston, E. Di Fabrizio, C. Ricciardi, Role of tensile stress in DNA Nanoresonators for epigenetic studies, ACS Appl. Nano Mater. 7 (2024), https://doi.org/10.1021/acsanm.4c01730.
[49] M. Marini, A. Falqui, M. Moretti, T. Limongi, M. Allione, A. Genovese, S. Lopatin, L. Tirinato, G. Das, B. Torre, A. Giugni, F. Gentile, P. Candeloro, E. Di Fabrizio, The structure of DNA by direct imaging, Sci. Adv. 1 (2015) e1500734, https://doi.org/10.1126/sciadv.1500734.
[50] M. Marini, G. Das, R. La Rocca, F. Gentile, T. Limongi, S. Santoriello, A. Scarpellini, E. Di Fabrizio, Raman spectroscopy for detection of stretched DNAs on superhydrophobic surfaces, Microelectron. Eng. 119 (2014) 151–154, https://doi.org/10.1016/j.mee.2014.04.008.
[51] D. Daniels, Complete Annotated Lambda Sequence, Lambda II (1983). https://cir.nii.ac.jp/crid/1571417124426217216 (accessed February 6, 2025).
[52] M. Marini, T. Limongi, A. Falqui, A. Genovese, M. Allione, M. Moretti, S. Lopatin, L. Tirinato, G. Das, B. Torre, A. Giugni, F. Cesca, F. Benfenati, E. Di Fabrizio, Imaging and structural studies of DNA-protein complexes and membrane ion channels, Nanoscale 9 (2017), https://doi.org/10.1039/c6nr07958j.
[53] M. Allione, T. Limongi, M. Marini, B. Torre, P. Zhang, M. Moretti, G. Perozziello, P. Candeloro, L. Napione, C.F. Pirri, E. Di Fabrizio, Micro/Nanopatterned Superhydrophobic surfaces fabrication for biomolecules and biomaterials manipulation and analysis, Micromachines 12 (2021) 1501, https://doi.org/10.3390/mi12121501.
[54] M. Marini, M. Allione, S. Lopatin, M. Moretti, A. Giugni, B. Torre, E. di Fabrizio, Suspended DNA structural characterization by TEM diffraction, Microelectron. Eng. 187–188 (2018) 39–42, https://doi.org/10.1016/j.mee.2017.11.020.
[55] P. Zhang, M. Moretti, M. Allione, Y. Tian, J. Ordonez-Loza, D. Altamura, C. Giannini, B. Torre, G. Das, E. Li, S.T. Thoroddsen, S.M. Sarathy, I. Autiero, A. Giugni, F. Gentile, N. Malara, M. Marini, E. Di Fabrizio, A droplet reactor on a super-hydrophobic surface allows control and characterization of amyloid fibril growth, Commun. Biol. 3 (2020) 457, https://doi.org/10.1038/s42003-020-01187-7.
[56] M. Moretti, M. Allione, M. Marini, B. Torre, A. Giugni, T. Limongi, G. Das, E. Di Fabrizio, Raman study of lysozyme amyloid fibrils suspended on super-hydrophobic surfaces by shear flow, Microelectron. Eng. 178 (2017), https://doi.org/10.1016/j.mee.2017.05.045.
[57] M. Moretti, T. Limongi, C. Testi, E. Milanetti, M.T. De Angelis, E.I. Parrotta, S. Scalise, G. Santamaria, M. Allione, S. Lopatin, B. Torre, P. Zhang, M. Marini, G. Perozziello, P. Candeloro, C.F. Pirri, G. Ruocco, G. Cuda, E. Di Fabrizio, Direct visualization and identification of membrane voltage-gated sodium channels from human iPSC-derived neurons by multiple imaging and light enhanced spectroscopy, Small Methods 6 (2022) 2200402, https://doi.org/10.1002/smtd.202200402.
[58] C.A. Lieber, A. Mahadevan-Jansen, Automated method for subtraction of fluorescence from biological Raman spectra, Appl. Spectrosc. 57 (2003) 1363–1367, https://doi.org/10.1366/000370203322554518.
[59] J.G. Duguid, V.A. Bloomfield, J.M. Benevides, G.J.J. Thomas, Raman spectroscopy of DNA-metal complexes. II. The thermal denaturation of DNA in the presence of Sr2+, Ba2+, Mg2+, Ca2+, Mn2+, Co2+, Ni2+, and Cd2+, Biophys. J. 69 (1995) 2623–2641, https://doi.org/10.1016/S0006-3495(95)80133-5.
[60] J.-P. Macquet, J.-L. Butour, A circular dichroism study of DNA. Platinum complexes. differentiation between monofunctional. cis-bidentate and trans-bidentate platinum fixation on a series of DNAs, Eur. J. Biochem. 83 (1978) 375–387, https://doi.org/10.1111/j.1432-1033.1978.tb12103.x.
[61] J. Kypr, I. Kejnovska, D. Renciuk, M. Vorlickova, Circular dichroism and conformational polymorphism of DNA, Nucleic Acids Res. 37 (2009) 1713–1725, https://doi.org/10.1093/nar/gkp026.
[62] F. Gentile, M. Moretti, T. Limongi, A. Falqui, G. Bertoni, A. Scarpellini, S. Santoriello, L. Maragliano, R. Proietti Zaccaria, E. Di Fabrizio, Direct imaging of DNA fibers: the visage of double helix, Nano Lett. 12 (2012) 6453–6458, https://doi.org/10.1021/nl3039162.
[63] J.D. Watson, F.H.C. Crick, Molecular structure of nucleic acids, Nature 171 (1953) 737–738, https://doi.org/10.1097/BLO.0b013e3181468780.
[64] M.H.F. Wilkins, A.R. Stokes, H.R. Wilson, Molecular structure of deoxypentose nucleic acids, Nature 171 (1953) 738–740, https://doi.org/10.1038/171738a0.
[65] M.P.M. Marques, D. Gianolio, G. Cibin, J. Tomkinson, S.F. Parker, R. Valero, R. P. Lopes, L.A.E.B. de Carvalho, A molecular view of cisplatin's mode of action: interplay with DNA bases and acquired resistance, Phys. Chem. Chem. Phys. 17 (2015) 5155–5171, https://doi.org/10.1039/C4CP05183A.
[66] D. Serban, J.M. Benevides, G.J. Thomas, DNA secondary structure and Raman markers of supercoiling in Escherichia coli plasmid pUC19, Biochemistry 41 (2002) 847–853, https://doi.org/10.1021/bi011004z.
[67] K.M. Šišková, Cisplatin interacting with buffering media and cysteine: molecular insight due to Raman microspectroscopy, J. Raman Spectrosc. 50 (2019) 528–536, https://doi.org/10.1002/jrs.5545.
[68] S. Olsztyńska-Janus, M. Gąsior-Głogowska, K. Szymborska-Małek, M. Komorowska, W. Witkiewicz, C. Pezowicz, S. Szotek, M. Kobielarz, Spectroscopic techniques in the study of human tissues and their components. Part II: Raman spectroscopy, Acta of Bioeng. Biomech. (2012), https://doi.org/10.5277/ABB120414, 04/2012; ISSN 1509-409X.
[69] E.B. Brown, W.L. Peticolas, Conformational geometry and vibrational frequencies of nucleic acid chains, Biopolymers 14 (1975) 1259–1271, https://doi.org/10.1002/bip.1975.360140614.
[70] E. Lipiec, A. Japaridze, J. Szczerbiński, G. Dietler, R. Zenobi, Preparation of well-defined DNA samples for reproducible Nanospectroscopic measurements, Small 12 (2016) 4821–4829, https://doi.org/10.1002/smll.201601711.

[71] J. Stangret, R. Savoie, Vibrational spectroscopic study of the interaction of metal ions with diethyl phosphate, a model for biological systems, Can. J. Chem. 70 (1992) 2875–2883, https://doi.org/10.1139/v92-367.
[72] P.A. Terpstra, C. Otto, G.M.J. Segers-Nolten, J.S. Kanger, J. Greve, Raman depolarization ratios in RNA and DNA are sensitive for sugar-base coupling, Biospectroscopy 1 (1995) 255–263, https://doi.org/10.1002/bspy.350010404.
[73] Y. Guan, C.J. Wurrey, G.J. Thomas, Vibrational analysis of nucleic acids. I. The phosphodiester group in dimethyl phosphate model compounds: (CH3O)2PO2-, (CD3O)2PO2-, and (13CH3O)2PO2-, Biophys. J. 66 (1994) 225–235, https://doi.org/10.1016/S0006-3495(94)80767-2.
[74] J.M. Benevides, A.H.J. Wang, G.A. Van der Marel, J.H. Van Boom, G.J. Thomas, Crystal and solution structures of the B-DNA dodecamer d(CGCAAATTTGCG) probed by Raman spectroscopy: heterogeneity in the crystal structure does not persist in the solution structure, Biochemistry 27 (1988) 931–938, https://doi.org/10.1021/bi00403a014.
[75] J. Kundu, O. Neumann, B.G. Janesko, D. Zhang, S. Lal, A. Barhoumi, G.E. Scuseria, N.J. Halas, Adenine− and adenosine monophosphate (AMP)−gold binding interactions studied by surface-enhanced Raman and infrared spectroscopies, J. Phys. Chem. C 113 (2009) 14390–14397, https://doi.org/10.1021/jp903126f.
[76] L. Movileanu, J.M. Benevides, G.J. Thomas Jr., Temperature dependence of the raman spectrum of DNA. II. Raman signatures of premelting and melting transitions of poly(dA)·poly(dT) and comparison with poly(dA-dT)·poly(dA-dT), Biopolymers 63 (2002) 181–194, https://doi.org/10.1002/bip.10022.
[77] M. Tsuboi, M. Komatsu, J. Hoshi, E. Kawashima, T. Sekine, Y. Ishido, M.P. Russell, J.M. Benevides, G.J. Thomas, Raman and infrared spectra of (2'S)-[2'-2H] thymidine: vibrational coupling between deoxyribosyl and thymine moieties and structural implications, J. Am. Chem. Soc. 119 (1997) 2025–2032, https://doi.org/10.1021/ja962676t.
[78] K.L. Aubrey, S.R. Casjens, G.J. Jr, Thomas, secondary structure and interactions of the packaged dsDNA genome of bacteriophage P22 investigated by Raman difference spectroscopy, Biochemistry 31 (1992) 11835–11842, https://doi.org/10.1021/bi00162a023.
[79] L. Movileanu, J.M. Benevides, G.J. Thomas, Temperature dependence of the raman spectrum of DNA. Part I—Raman signatures of premelting and melting transitions of poly(dA-dT)·poly(dA-dT), J. Raman Spectrosc. 30 (1999) 637–649, https://doi.org/10.1002/(SICI)1097-4555(199908)30:8<637::AID-JRS431>3.0.CO;2-B.
[80] M.J. Lane, G.J. Thomas, Kinetics of hydrogen-deuterium exchange in guanosine 5′-monophosphate and guanosine 3′:5′-monophosphate determined by laser-Raman spectroscopy, Biochemistry 18 (1979) 3839–3846, https://doi.org/10.1021/bi00585a002.
[81] L. Movileanu, J.M. Benevides, G.J. Thomas Jr., Determination of base and backbone contributions to the thermodynamics of premelting and melting transitions in B DNA, Nucleic Acids Res. 30 (2002) 3767–3777, https://doi.org/10.1093/nar/gkf471.
[82] Y. Nishimura, M. Tsuboi, T. Nakano, S. Higuchi, T. Sato, T. Shida, S. Uesugi, E. Ohtsuka, M. Ikehara, Raman diagnosis of nucleic acid structure: sugar-puckering and glycosidic conformation in the guanosine moiety, Nucleic Acids Res. 11 (1983) 1579–1588, https://doi.org/10.1093/nar/11.5.1579.
[83] K. Serec, N. Šegedin, M. Krajačić, S. Dolanski Babić, Conformational transitions of double-stranded DNA in thin films, Appl. Sci. 11 (2021) 2360, https://doi.org/10.3390/app11052360.
[84] J. Ruiz-Chica, M.A. Medina, F. Sánchez-Jiménez, F.J. Ramírez, Fourier transform Raman study of the structural specificities on the interaction between DNA and biogenic polyamines, Biophys. J. 80 (2001) 443–454, https://doi.org/10.1016/S0006-3495(01)76027-4.
[85] A. Rasmussen, V. Deckert, Surface- and tip-enhanced Raman scattering of DNA components, J. Raman Spectrosc. 37 (2006) 311–317, https://doi.org/10.1002/jrs.1480.
[86] A.J. Ruiz-Chica, M.A. Medina, F. Sánchez-Jiménez, F.J. Ramírez, On the interpretation of Raman spectra of 1-aminooxy-spermine/DNA complexes, Nucleic Acids Res. 32 (2004) 579–589, https://doi.org/10.1093/nar/gkh232.
[87] O.P. Lamba, R. Becka, G.J. Thomas Jr., Adenine and guanine 8CH exchange in nucleic acids: resolution and measurement by Raman optical multichannel analysis, Biopolymers 29 (1990) 1465–1477, https://doi.org/10.1002/bip.360291013.
[88] E.A. Zubova, I.A. Strelnikov, Experimental detection of conformational transitions between forms of DNA: problems and prospects, Biophys. Rev. 15 (2023) 1053–1078, https://doi.org/10.1007/s12551-023-01143-9.
[89] W. Saenger, W.N. Hunter, O. Kennard, DNA conformation is determined by economics in the hydration of phosphate groups, Nature 324 (1986) 385–388, https://doi.org/10.1038/324385a0.
[90] J.Y. Lee, T.-H. Lee, Effects of DNA methylation on the structure of nucleosomes, J. Am. Chem. Soc. 134 (2012) 173–175, https://doi.org/10.1021/ja210273w.
[91] S. Rao, T.-P. Chiu, J.F. Kribelbauer, R.S. Mann, H.J. Bussemaker, R. Rohs, Systematic prediction of DNA shape changes due to CpG methylation explains epigenetic effects on protein–DNA binding, Epigenetics Chromatin 11 (2018) 6, https://doi.org/10.1186/s13072-018-0174-4.
[92] H.S. Basu, H.C.A. Schwietert, B.G. Feuerstein, L.J. Marton, Effects of variation in the structure of spermine on the association with DNA and the induction of DNA conformational changes, Biochem. J. 269 (1990) 329–334, https://doi.org/10.1042/bj2690329.